Evidence of Extensive Intraspecific Noncoding Reshuffling in a 169-kb Mitochondrial Genome of a Basidiomycetous Fungus

Hsin-Han Lee [1], Huei-Mien Ke [1], Chan-Yi Ivy Lin [1], Tracy J. Lee [1,2,3], Chia-Lin Chung [4], and Isheng J. Tsai [1,*]

[1]Biodiversity Research Center, Academia Sinica, Taipei City, Taiwan

[2]Biodiversity Program, Taiwan International Graduate Program, Academia Sinica and National Taiwan Normal University, Taipei City, Taiwan

[3]Department of Life Science, National Taiwan Normal University, Taipei City, Taiwan

[4]Department of Plant Pathology and Microbiology, National Taiwan University, Taipei City, Taiwan

*Corresponding author: E-mail: ijtsai@sinica.edu.tw.

Accepted: August 13, 2019

Data deposition: This project has been deposited at NCBI under the accession CM008263 and MK623257–MK623261.

Abstract

Comparative genomics of fungal mitochondrial genomes (mitogenomes) have revealed a remarkable pattern of rearrangement between and within major phyla owing to horizontal gene transfer and recombination. The role of recombination was exemplified at a finer evolutionary time scale in basidiomycetes group of fungi as they display a diversity of mitochondrial DNA inheritance patterns. Here, we assembled mitogenomes of six species from the *Hymenochaetales* order of basidiomycetes and examined 59 mitogenomes from 2 genetic lineages of *Phellinus noxius*. Gene order is largely collinear, while intergene regions are major determinants of mitogenome size variation. Substantial sequence divergence was found in shared introns consistent with high horizontal gene transfer frequency observed in yeasts, but we also identified a rare case where an intron was retained in five species since speciation. In contrast to the hyperdiversity observed in nuclear genomes of *Phellinus noxius*, mitogenomes' intraspecific polymorphisms at protein-coding sequences are extremely low. Phylogeny network based on introns revealed turnover as well as exchange of introns between two lineages. Strikingly, some strains harbor a mosaic origin of introns from both lineages. Analysis of intergenic sequence indicated substantial differences between and within lineages, and an expansion may be ongoing as a result of exchange between distal intergenes. These findings suggest that the evolution in mitochondrial DNAs is usually lineage specific but chimeric mitotypes are frequently observed, thus capturing the possible evolutionary processes shaping mitogenomes in a basidiomycete. The large mitogenome sizes reported in various basidiomycetes appear to be a result of interspecific reshuffling of intergenes.

Key words: mitochondrial evolution, mitogenome size variation, population mitogenomics, mitogenomics.

Introduction

A typical fungal mitochondrial genome (mitogenome) consists of a circular DNA, which encodes 14 mitochondrial-exclusive protein-coding genes, ribosomal RNAs and transfer RNAs usually in clusters (Férandon et al. 2013; Aguileta et al. 2014; Sandor et al. 2018). Depending on groups, these elements are encoded either on the same strand in ascomycetous or on both in basidiomycetous mitogenomes (Aguileta et al. 2014). These genomes are highly diversified in size ranging from 19,431 bp in *Schizosaccharomyces pombe* (Bullerwell et al. 2003) to 235,849 bp in *Rhizoctonia solani* (Losada et al. 2014). Variations in mitogenome size can be large among species within a genus (Bullerwell et al. 2003) or among strains of the same species (Wolters et al. 2015). Presence and expansion of introns in mitogenome protein encoding genes as well as sizable noncoding regions (NCRs) are major determinants of fungal mitogenome size variations (Xu and Wang 2015; Sandor et al. 2018). Given that the highly variable nature of fungal mitogenome size, characterizing the dynamics of introns and determining the origin and function of these NCRs is critical for understanding the evolution of fungal mitogenome.

Inheritance of mitochondrial DNA (mtDNA) is predominantly maternal in sexual plants and animals (Xu

and Wang 2015; Sandor et al. 2018). In the Fungi kingdom, however, alternative modes of inheritance have been commonly reported during sexual reproduction (Berger and Yaffe 2000; Basse 2010; Wilson and Xu 2012; Xu and Wang 2015). For instance, the model ascomycete yeasts, *Saccharomyces cerevisiae* and *Schizosaccharomyces pombe*, are known to inherit mitochondria biparentally (Wolf et al. 1976; Basse 2010; Xu and Wang 2015). The zygote contains mtDNA from both parents and subsequently segregated into homoplasmic progenies through the process of syngamy. Like animals and plants, the mating process in filamentous ascomycetes usually initiated with the fusion of two morphologically different gametes, and the mitochondria are typically inherited from the larger gamete (Sandor et al. 2018). For basidiomycetes, various modes of mitochondrial inheritance may have been involved in generating recombinant mitochondrial genotypes (Xu and He 2015; Xu and Wang 2015; Sandor et al. 2018).

In fungi, tight regulation of mtDNA transmission is part of molecular mechanisms responsible for sex determination (mating). For model basidiomycetes yeast *Cryptococcus neoformans*, mtDNA is inherited uniparentally from *MAT*a parent but becomes biparental if the sex-specific homeodomain transcription factors *sxi1α* and *sxi2a* are disrupted (Xu et al. 2000; Yan and Xu 2003). A closely related species of *Cryptococcus neoformans*, *Cryptococcus gattii* exhibited different inheritance patterns depending on strain combinations and environmental factors such as temperature (Voelz et al. 2013; Zhu et al. 2013; Wang et al. 2015). For *Ustilago maydis*, which has a tetrapolar mating system similar to the model mushroom *Coprinopsis cinerea*, the mtDNA inheritance is controlled by *lga2* and *rga2* of uncertain function encoded by *a2* locus (homologous to *C. cinerea matB* locus) (Fedler et al. 2009).

Strictly selecting mtDNA from only one parent during mating ensures uniparental inheritance. This is the case for model filamentous basidiomycetes such as *C. cinerea* and *Schiozphyllum commune*, where the formation of diploid involves nuclear but not mitochondrial migration, resulting in genetically identical dikaryons with different mitochondria from either parent (Sandor et al. 2018). Nuclear migration is controlled by *matB* locus encoding peptide pheromones and pheromone receptors (Casselton and Kües 2007), again indicating a strong correlation between mating locus and mitochondria inheritance. Alternatively, the button mushroom *Agaricus bisporus* and many basidiomycetes do not undergo nuclear migration and clamp formation; instead, they undergo direct hyphal fusion during mating process. This means different mitochondrial genotypes can be present within hyphal cells, suggesting the opportunity to exchange DNA via mitochondrial recombination. Indeed, *A. bisporus* is known to have uniparental and nonparental mitochondrial inheritance patterns (Hintz et al. 1988; Jin and Horgen 1993, 1994; de la Bastide and Horgen 2003) and have displayed signatures of recombination in natural populations (Xu et al. 2013). Hence, the ephemeral diploid phase may be particularly important in mitochondrial inheritance and diversity (de la Bastide and Horgen 2003; Xu and Wang 2015).

Among the estimated 2.2–3.8 million fungal species (Hawksworth and Lücking 2017), many lineages still lack a formal description or analysis of mitogenomes. One interesting case is the order *Hymenochaetales* (*Agaricomycetes*, *Basidiomycota*), which is dominated by wood decay fungi. Most species in this order are saprotrophic, but some are pathogens involved in major forest incidents since 1971 in different parts of the world (Hepting 1971; Sahashi et al. 2012). In particular, *Phellinus noxius* has a very wide host range, spanning more than 200 broadleaved and coniferous tree species (at least 59 families), and are the causative agents responsible for brown root rot disease in parts of Asia (Akiba et al. 2015; Chung et al. 2015). A recent comparative and population genomics study of six genomes from this order and 60 *P. noxius* strains from Taiwan and Japan revealed that *P. noxius* possesses extraordinarily high diversity in its nuclear genomes (Chung et al. 2017).

Phellinus noxius lacks clamp connections (Ann et al. 2002) and displays a bipolar heterothallic mating system (Chung et al. 2017) with a highly expanded A locus spanning a ~60-kb region. The availability of whole genome sequences of *P. noxius* populations prompted us to further understand the evolution of mitogenomes in this hypervariable species. In this study, we first assembled and compared the mitogenomes of *P. noxius* and five *Hymenochaetales* species. We demonstrated that core genes are largely in syntenic across these species while both introns and NCRs constitute the majority of *P. noxius* mtDNA. We then examined mitogenome evolution from two genetically independent lineages of *P. noxius* and discovered frequent rearrangement in NCRs. The main purpose of this study was to elucidate possible mechanisms driving mitogenome enlargement in *P. noxius* at a population level. We provided evidences of frequent mitochondrial exchange possibly in heteroplasmy stage during hyphal fusion and mating resulting in recombinant mitotype and expanding mitogenome.

Materials and Methods

De Novo Assembly or Reconstruction of Four *Hymenochaetales* Mitochondrial Genomes

Sequencing data of *P. noxius*, *Phellinus lamaensis*, *Porodaedalea pini*, and *Coniferiporia sulphurascens* (syn. *Phellinus sulphurascens*) were described in Chung et al. (2017). Mitochondrial genomes (mitogenomes) were assembled in 1–6 iterations using Organelle_PBA (v1.0.7; Soorni et al. 2017) with PacBio reads until sequence circularity was detected. Partial mtDNA sequence in the published assembly of each species or conserved protein-coding gene was used as initial reference for the first run. Illumina sequencing data of

Fomitiporia mediterranea (Floudas et al. 2012) were obtained from Joint Genome Institute (JGI) database (https://genome.jgi.doe.gov/Fomme1/Fomme1.home.html). The *F. mediterranea* mitogenome was assembled using NOVOplasty (v2.6.7; Dierckxsens et al. 2017) with *Po. pini*'s mitogenome as the seed sequence. Circularity was assessed either by in-built function in the assemblers or subsequently by "check_circularity.pl" script distributed with sprai de novo assembly tool (v0.9.9.23; http://zombie.cb.k.u-tokyo.ac.jp/sprai). The consensus of assemblies was improved using pilon (v1.22; Walker et al. 2014). The complete mitogenome of *Schizopora paradoxa* (Min et al. 2015) is available in JGI database (https://genome.jgi.doe.gov/Schpa1/Schpa1.home.html) and was retrieved for further annotation and analysis.

Annotation of Mitogenomes

Core genes in mitogenomes were annotated using MFannot web service (http://megasun.bch.umontreal.ca/cgi-bin/mfannot/mfannotInterface.pl) with genetic code table 4. Exon boundaries were further manually curated based on multiple sequence alignment of homologs from closely related species using MUSCLE (v3.8.31; Edgar 2004) and RNA-seq alignments where available. tRNA genes were predicted by MFannot, tRNAscan-SE (v2.0; Lowe and Chan 2016), and Aragorn (v1.2.38; Laslett and Canbäck 2004). Only tRNA positions supported by at least two programs were retained for further analysis. Putative open reading frames (ORFs) were predicted by NCBI ORFfinder (v0.4.3; Wheeler et al. 2003) against exon-masked mitogenomes, and hypothetical proteins were searched against Pfam (Finn et al. 2016) and NCBI protein nr database (https://www.ncbi.nlm.nih.gov/protein) for evidence of homing endonuclease (HE) and DNA/RNA polymerase (dpo/rpo) genes. Introns were assigned into subgroups using RNAfinder (v1.40; https://github.com/BFL-lab/RNAfinder). Putative HE domains in introns were searched by PfamScan (v31; Finn et al. 2016). Direct and palindromic repeats were searched using Vmatch (v2.3.0; http://www.vmatch.de) with parameters of "-seedlength 30 -l 30 -exdrop 3 -identity 80." Tandem repeats were identified using Tandem Repeat Finder (v4.09; Benson 1999) with default parameters. Analysis of simple sequence repeats were performed by MISA (v2.0; Thiel et al. 2003) with default parameters.

RNA Sequencing

The mycelia of *P. noxius* KPN91 were cultured on the PDA agar plates at 25 °C for about 3–5 days. Total RNA was extracted from mycelia homogenized in liquid nitrogen, following with TRIzol Reagent (catalog no. 15596018, Thermo Fisher Scientific, Inc.). Ploy-A enriched RNA (200 ng) was purified from total RNA by using Dynabeads mRNA purification kit (catalog no. 61006, Thermo Fisher Scientific, Inc.) and was used to conduct cDNA library preparation with Direct cDNA Sequencing kit (SQK-DCS108; Oxford Nanopore Technologies). The reads were sequenced with FLO-MIN106 flow cell on a GridION, Oxford Nanopore and then basecalled by dogfish v0.9.3. Illumina RNA-seq reads of four species in this study (*P. noxius*, *P. lamaensis*, *Po. pini*, and *Con. sulphurascens*) were downloaded and aligned to corresponding assemblies using STAR (v2.6.0a; Dobin et al. 2013). Nanopore cDNA reads (*P. noxius*) were aligned using minimap2 (v2.6; Li 2018). Only reads aligned to mitogenome were retained for further analysis.

Assembly and Annotation of *P. noxius* Isolates

The sequencing data of a total of 59 *P. noxius* isolates were described in a previous study (Chung et al. 2017). All of the mitogenomes were assembled using the same pipeline with *F. mediterranea* as described above except that the seed sequence was *P. noxius* KPN91 mitogenome. Annotation of core genes was searched with query of curated genes of KPN91 using GMAP (v2017-11-15; Wu and Watanabe 2005), followed by multiple sequence alignment using MUSCLE (v3.8.31; Edgar 2004) to identify precise exon–intron boundaries. tRNA annotation was processed as described above. The four (three "large" ranging 6.3–35.4 kb and a small 4.6–8.9 kb) regions were defined and characterized by their frequently rearrangements when compared with KPN91 mtDNA reference (region 1: *nad4-rnl*, region 2: *atp8-cox1*, region 3: *nad5-rns*, and region 4s: *cox2-cob*).

Phylogenetic Analysis

Phylogenetic analysis of six *Hymenochaetales* species was carried out using concatenated amino acid alignments of 15 mitochondrial protein-coding genes by MUSCLE (v3.8.31; Edgar 2004), and pruned by trimal strict plus mode (v1.4; Capella-Gutierrez et al. 2009). A maximum-likelihood phylogeny was computed using iqtree (v1.6.6; Nguyen et al. 2015) with LG + F + I + G4 model and 100 bootstrap replicates. The same approach was used to produce the intron phylogeny for *P. noxius* isolates, except that ModelFinder (Kalyaanamoorthy et al. 2017) in iqtree was invoked to automatically determine the best-fit model. Maximum-likelihood distances inferred by iqtree were passed to SplitsTree4 program to generate a Neighbor-Net (NN) phylogenetic network of concatenated introns (Bryant and Moulton 2004). To validate the robustness of mitochondrial protein-coding genes phylogeny, four unpublished *Hymenochaetales* species available on JGI database (*Onnia scaura*, *Phellinus ferrugineofuscus*, *Porodaedalea chrysoloma*, and *Porodaedalea niemelaei*) were used to replot the phylogeny.

DNA Preparation and Polymerase Chain Reaction Condition

Genomic DNA of three isolates (KPN91, KPN323, and Pn113) for intergenic rearrangement validation were prepared as

described by Chung et al. (2017). Mitogenomes between these isolates were aligned using MUMmer (v4.0.0beta2; Kurtz et al. 2004) and primers were designed at the synteny blocks within predefined intergenic regions (1–3) using Primer3Plus web service (Untergasser et al. 2012). The primers were further filtered for nonspecificity by BlastN (v2.6.0; McGinnis and Madden 2004) against three mitogenomes. Each PCR composed of ~10-ng template DNA, 10 μl KAPA HiFi HotStart ReadyMix (2×) (0.4 U of DNA polymerase, $MgCl_2$ at a final concentration of 2.5 mM, each dNTP at a final concentration of 0.3 mM) (Kapa Biosystems), 0.3 μM of each primer, and sterilized distilled water to make up a total volume of 20 μl. Thermo cycling profile included an initial denaturing temperature of 95 °C for 3 min followed by 35 cycles of 98 °C for 20 s, 60 °C for 15 s (for A1_F/B1_R and A1_F/rnl_R using 65 °C, and for F1_F/C1_R and apt8_F/C1_R using 62 °C), and 72 °C for 1 min per kb. The final extension step was 72 °C for 1 min per kb. The PCR products were then analyzed by electrophoresis on 1% agarose gel at 70 V for 45 min. The primer sequences are listed in supplementary table S4, Supplementary Material online.

Pairwise Identity Calculation

Intergenic sequences of four predefined regions were aligned separately using MAFFT (v7.310; Katoh and Standley 2013) with parameters of "–ep 0 –genafpair" to incorporate large indels. The aligned sequences were then concatenated for identity calculation. Direct identity was referred to matched bases over alignment length, and gap-compressed method counted gaps regardless of length as one difference, therefore reduced the extent of large indels on identity score.

Prediction and Significance Test of Rearrangement Breakpoints

All 58 mitogenomes were aligned against KPN91 reference using MUMmer (v4.0.0beta2; Kurtz et al. 2004) to identify the breakpoints of rearrangement segments. A rearrangement segment was defined according to one of the following rules: 1) rearrange across different intergenic regions, 2) rearrange within a single intergenic region, and 3) inversion (supplementary fig. S8, Supplementary Material online). The breakpoints were the boundaries of rearrangement segments and the isolates with <10 breakpoints were omitted. To test the correlation between breakpoints and repetitive elements, we sampled equal number of positions within predefined intergenic regions and the probability of breakpoints locating on repetitive elements was calculated. One thousand bootstrap replicates were performed to infer adjusted *P* values. The analyses were conducted with python scripting language.

Results

Assembly and Annotation of Six *Hymenochaetales* Mitochondrial Genomes

There are two published mitogenomes in *Hymenochaetales* species, with genome size ranging from 57.5 kb in *S. paradoxa* (Min et al. 2015) to 163.4 kb in *P. noxius* (Chung et al. 2017). Such large differences in mitogenome sizes prompted us to assemble four more *Hymenochaetales* species using available Illumina or Pacbio long sequences: *P. lamaensis*, *Po. pini*, *Con. sulphurascens*, and *F. mediterranea*. The four *Hymenochaetales* mitogenomes now range from 45.6 to 145.0 kb (table 1), again showing high variations. GC content are low (23.4–34.6%), consistent with the AT-rich nature of fungal mitogenomes (Hausner 2003). Remapping of Illumina reads against the mitogenomes showed no heterozygosity, suggesting that mitogenomes are homozygous in these species with no evidence of heteroplasmy. All six species were predicted to contain 15 protein-coding genes and 2 ribosomal RNA genes (fig. 1 and supplementary figs. S1 and S2*A*, Supplementary Material online). Twenty-five tRNAs encoding 20 standard amino acids were shared across 6 species and positioned into 3–5 clusters, with the presence of 1–2 species-specific tRNA. All 17 core genes and tRNA clusters of 6 species are encoded on the same strand with an exception of a histidine tRNA in *S. paradoxa* (supplementary fig. S1*E*, Supplementary Material online). Interestingly, in four *Hymenochaetales* species, *nad5* starts (ATG) immediately from the last base of adjacent *nad4L* stop codon (TAA), which has been observed in various fungal mitochondria (Férandon et al. 2013; Wang et al. 2018).

Coding contents are relatively conserved across the six *Hymenochaetales* species (average 22.5 kb), however, huge variations were observed in their intronic and intergenic sequences. Prediction of ORFs in intronic and intergenic regions resulted in 18–100 putative protein-coding sequences (table 1 and supplementary table S1, Supplementary Material online). Majority of the ORFs did not show homology across various databases. The ORFs with confident protein domain profiles assigned were mostly HE (containing LAGLIDADG or GIY-YIG domain) and family B DNA polymerase (*dpoB*). *Phellinus noxius* has the largest mitogenome among the six *Hymenochaetales* species, with 38.2% introns and 48.4% intergene sequences. The mitogenome of *Po. pini* has an intron content of 17.5% and 65.7% intergene region. In contrast, *P. lamaensis* has the most reduced mitogenome with highest percentage of coding content (46.8%). We further investigated whether repetitive sequences contributed to the noncoding content of these mitogenomes. The total repeat content accounted for 2.9–8.5% of mitogenomes, with only two large palindromic repeats (>500 bp) observed in *Po. pini*. These repeats did not contribute to the majority of noncoding content as only 4.7–12.2% of intergenic sequences were classified as repetitive. The invertron-like sequences are plasmids

Table 1
General Statistics of Six Mitogenomes

Species	*P. noxius*	*P. lamaensis*	*Po. pini*	*F. mediterranea*	*Con. sulphurascens*	*S. paradoxa*
Coverage (Pacbio)	2,860	6,175	2,673	—	6,477	—
Coverage (Illumina)	744	3,873	555	1,116	1,021	—
Mitogenome length	163,449	45,604	144,970	115,036	58,959	57,732
GC content (%)	28.68	34.55	28.26	23.39	33.17	28.22
# tRNAs	27	26	26	27	25	26
# Exons of 17 standard genes	78	20	38	45	18	25
atp6	1	1	1	1	1	1
atp8	1	1	1	1	1	1
atp9	1	1	1	1	1	1
cob	9	3	3	6	2	2
cox1	24	2	12	13	1	7
cox2	5	1	1	3	1	1
cox3	3	1	1	2	1	1
nad1	5	1	1	3	1	1
nad2	2	1	1	1	1	1
nad3	1	1	1	1	1	1
nad4	2	1	1	2	1	1
nad4L	1	1	1	1	1	1
nad5	7	1	2	3	1	1
nad6	1	1	1	1	1	1
rps3	1	1	1	1	1	1
rnl	13	1	8	4	1	2
rns	1	1	1	1	1	1
# Introns	61	3	21	28	1	8
# ORFs	95	18	100	66	30	24
HEG[a]	21	2	15	22	0	6
dpoB[b]	3	1	11	4	5	1
Length of exons	21,975 (13.44%)	21,345 (46.81%)	24,328 (16.78%)	22,242 (19.33%)	23,435 (39.75%)	21,795 (37.75%)
Length of introns	62,449 (38.21%)	2,829 (6.2%)	25,366 (17.5%)	34,228 (29.75%)	755 (1.28%)	8,733 (15.13%)
Length of intergene	79,025 (48.35%)	21,430 (46.99%)	95,276 (65.72%)	58,566 (50.91%)	34,769 (58.97%)	27,204 (47.12%)
Length of repeats	12,784 (7.82%)	1,588 (3.48%)	12,377 (8.54%)	3,771 (3.28%)	2,059 (3.49%)	1,685 (2.92%)

[a]Homing endonucleases containing LAGLIDADG or GIY-YIG domain.
[b]Family B DNA polymerase.

integrated into fungal or plant mtDNA, usually consisting of *dpoB* and DNA-dependent RNA polymerase between inverted repeats (Hausner 2012; Mardanov et al. 2014). Although intact invertron-like sequences were not observed, we found at least one *dpoB* gene in each mitogenome suggesting possible ancient integration events.

Gene Synteny

Species phylogeny inferred from 1,127 orthologous single copy genes placed species of similar genome sizes and primary habits together with *S. paradoxa* being the most diverged clade (Chung et al. 2017). The mitochondrial phylogeny of six *Hymenochaetales* was inferred from concatenation of 15 protein-coding genes (fig. 2). Different from the nuclear phylogeny, *Con. sulphurascens* was in the same clade with *Po. pini* and *F. mediterranea*. The gene order of 17 core genes and tRNA clusters were considerably conserved across five of the six *Hymenochaetales* species. For example, the largest synteny block started from *cox1* and extended to 22 genes (blue box). Greatest difference was found in *S. paradoxa*, which agrees with the nuclear phylogeny (Chung et al. 2017). In the clade of *P. noxius* and *P. lamaensis*, *nad4* and *rnl* genes were both relocated to downstream of t1 tRNA cluster. Furthermore, the location of t2 tRNA cluster and *rps3-atp8* block was swapped in *P. lamaensis*. Both *P. noxius* and *P. lamaensis* harbored a tRNA between *nad4* and *rnl*. The two tRNAs shared 88.9% identity in the 72-bp gene region, suggesting accumulation of mutations in a recently gained gene. Boundaries of intergenic spacers were similar between *P. noxius* and *P. lamaensis* but not across other species. Gene duplication events were only observed in t2 in *Po. pini* and t5 tRNA clusters in *F. mediterranea*.

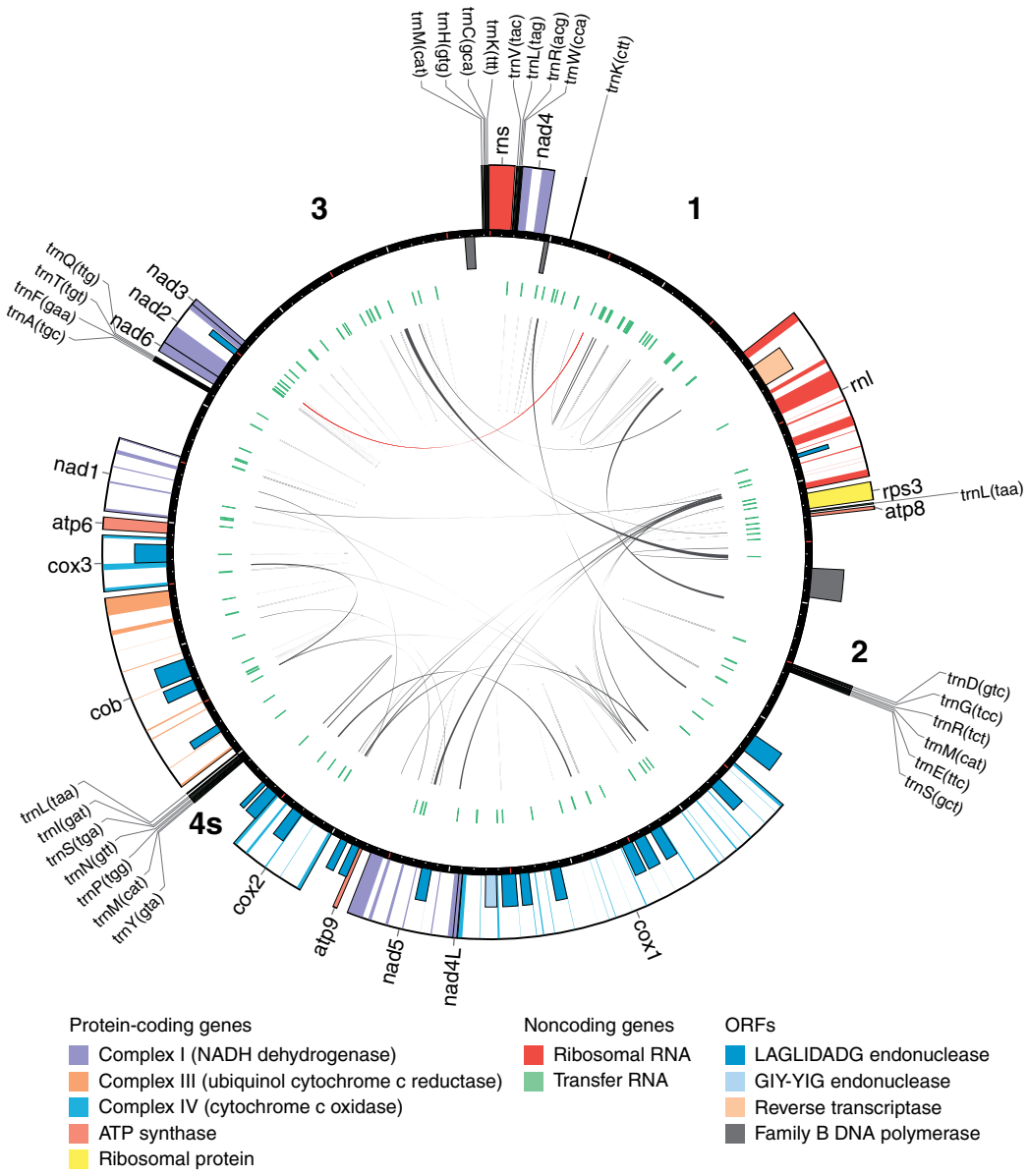

Fig. 1.—Genetic map of *Phellinus noxius* KPN91 mitogenome. The first base is defined as the start of *rns* gene. The ticks on the circle are separated by 1 kb. The boxes adhered to the circle are genes and the half-sized boxes are predicted ORFs. The boxes at outside and inside the circle indicates the genes encoding on positive and negative strand, respectively. Colored regions are exons. In the inner circle, green tiles represent the tandem repeats and the black and red links represent the direct and palindromic repeats, respectively. The bold numbers indicated the four defined intergenic regions (1–3 and 4s). The plot was generated using Circos software (Krzywinski et al. 2009).

Mitochondrial Intron Dynamics

Phellinus noxius mitogenome contains most introns in 6 species, with 61 introns spreading in 9 genes. In contrast, *Con. sulphurascens* mitogenome contains only one intron in *cob* gene. The largest reservoir of introns is *P. noxius cox1* gene, which retains 23 group I introns and a group II intron (17th intron), accounting for 93.5% of this gene. A total of 122 introns locating in 65 genetic sites were identified in six *Hymenochaetales* mitogenomes, with 39 sites were shared among species (fig. 3 and supplementary table S2, Supplementary Material online). No introns were found in eight genes (*atp6*, *atp8*, *atp9*, *nad3*, *nad4L*, *nad6*, *rns*, and *rps3*), whereas the *cob* gene contained at least one intron in every species. The majority of introns were of group I (114/122) and were classified into six subgroups (IA, IA3, IB, IC2, ID, and I-derived). Of these, group IB introns accounted for 57.4% of total introns (70/122). Interestingly, the 13th intron of *P. noxius* cox1 gene (cox1_intron13) was predicted to have

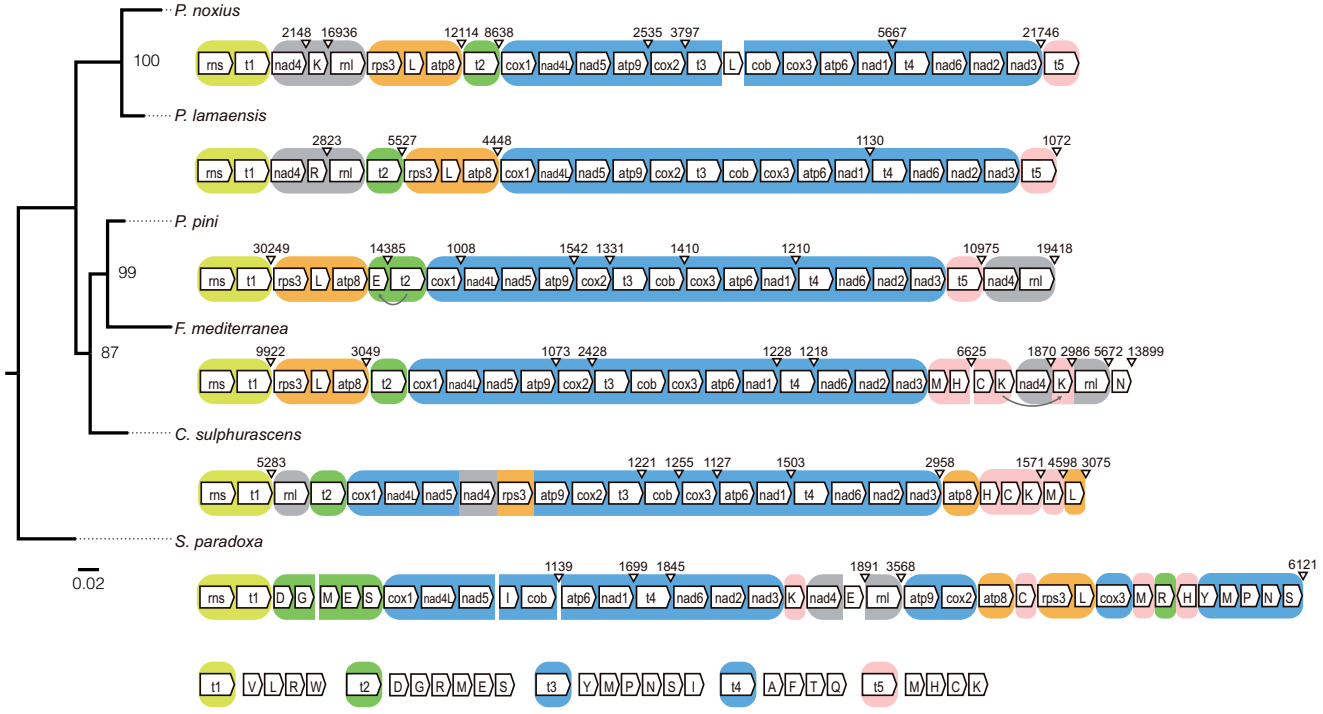

Fig. 2.—Phylogenetic tree of mitochondrial protein-coding genes and gene synteny in six mitogenomes. The colored boxes represent different conserved gene blocks. The intergene length larger than 1 kb is labeled above the gene wedges. The arrows below the gene wedges indicate gene duplication. The bootstrap values were inferred with 100 replicates.

two separated complete intron cores (IB and ID) suggesting a twintron: an intron inserted by another intron (Deng et al. 2018).

One possible explanation for the prevalence of introns in these species is the presence of HEs, which are highly specific endonucleases playing an important role in intron homing and precise splicing in group I introns (Yan et al. 2018). We searched for protein domains and ORFs, revealing that 65 introns each containing at least one LAGLIDADG or GIY-YIG domain. Nine of these introns did not have any predicted ORF suggesting loss of HE activity. Conversely, 12 intronic ORFs showed no evidence of HE domain. In addition to group I introns, we found 3 out of 5 group II introns comprising a putative LAGLIDADG domain, which has been reported in several filamentous fungi but showed no activity in enhancing splicing itself. LAGLIDADG domain might be an invaded group I HEG in a group II intron (Toor and Zimmerly 2002; Mullineux et al. 2010). Only a group II intron (PNOK_rnl_intron01) comprised an intact ORF with a complete reverse transcriptase domain.

Out of 39 intron sites present in multiple species, 34 comprised introns belonging to the same subgroup suggest a preference of insertion (Swithers et al. 2009). Alternatively, these introns may have already been inserted since their common ancestor; however, this may be less likely as the shared introns showed as low as 74.3% nucleotide identity. This scenario may be more likely in sites where introns are still found in more than three species. There are three such intron sites (cob_site5, cox1_site10, and cox1_site13) and phylogeny indicated two sites (cox1_site10 and cox1_site13) were concordant with the mitochondrial phylogeny, suggesting the intron was present since these species' common ancestor (supplementary fig. S3, Supplementary Material online).

Population Mitogenomics of *P. noxius*: General Characteristics

The mitogenomes of additional 58 *P. noxius* isolates from Japan and Taiwan region were assembled into single circular sequences using NOVOPlasty (supplementary table S3, Supplementary Material online). The mitogenome size can differ by 22 kb ranging from 146,191 bp of Pn102 to 168,365 bp of Pn120. A strong correlation was observed in intergenic region and mitogenome size (R^2 = 0.987, $P < 0.001$; fig. 4) but not exonic and intronic sequences (R^2 = 0.0213 and R^2 = 0.0203, respectively; fig. 4), suggesting that the expansion of mitochondria was mainly contributed by intergenic regions in *P. noxius*.

Low Intraspecific Polymorphism in Coding Regions

All 17 core genes were present in all isolates. Gene structures were highly conserved except for two protein-coding genes. Stop codon in the majority of isolates in the *cox2* gene was

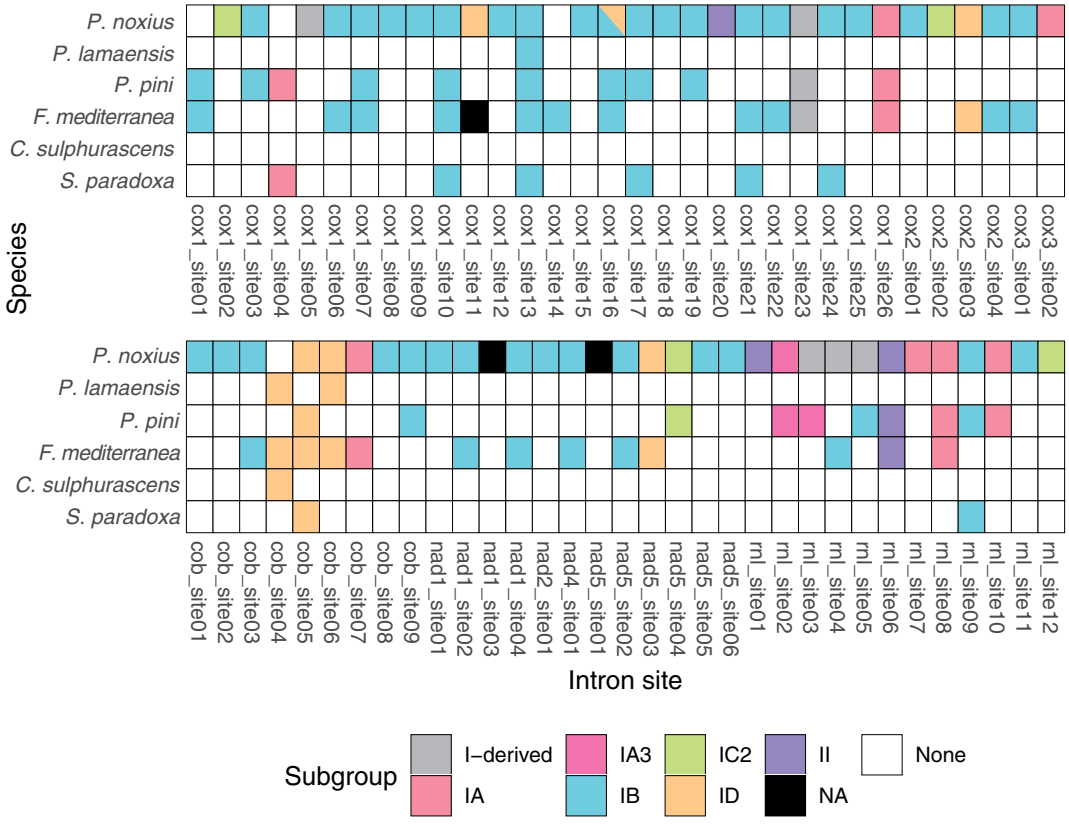

Fig. 3.—Shared intron positions and intron subgroups in six *Hymenochaetales* species. Details of intron properties refer to supplementary table S2, Supplementary Material online. NA: not assigned to any subgroup.

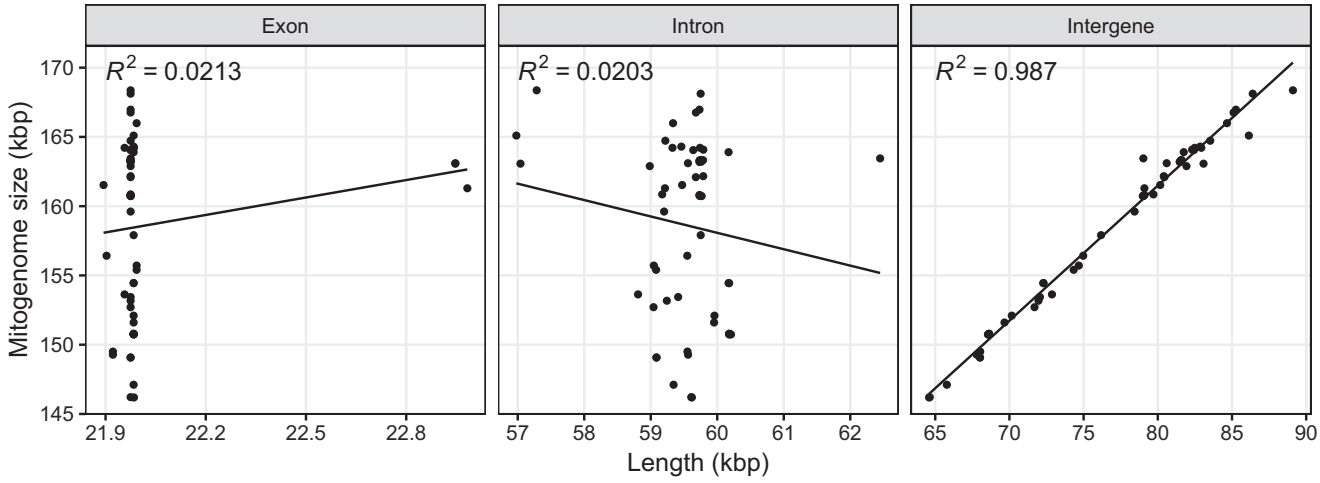

Fig. 4.—Correlation between mitogenome size and genome properties across 59 *Phellinus noxius* isolates. Each dot represents an isolate. Details refer to supplementary table S3, Supplementary Material online.

lost in three isolates with two possible changes (minor allele 1: KPN57 and Pn315; minor allele 2: Pn040). The prevalent allele encoded for a 765 bp *cox2* gene with five exons, and two minor alleles extended 972 and 1,008 bp in the last exon, respectively. In *nad2* gene, a tandem repeat [$(AGAAACTAA)_{3.8–7.8}$] located in the second exon varied the length of coding regions from 1,695 to 1,731 bp without interrupting the reading frame. Across 4,603 amino acid sites, only 13 and 7 were parsimony-informative and singletons, respectively (supplementary fig. S4, Supplementary Material online). Number of tRNA ranged from 26 to 27. A free-standing tRNA between *nad4* and *rnl* was found to

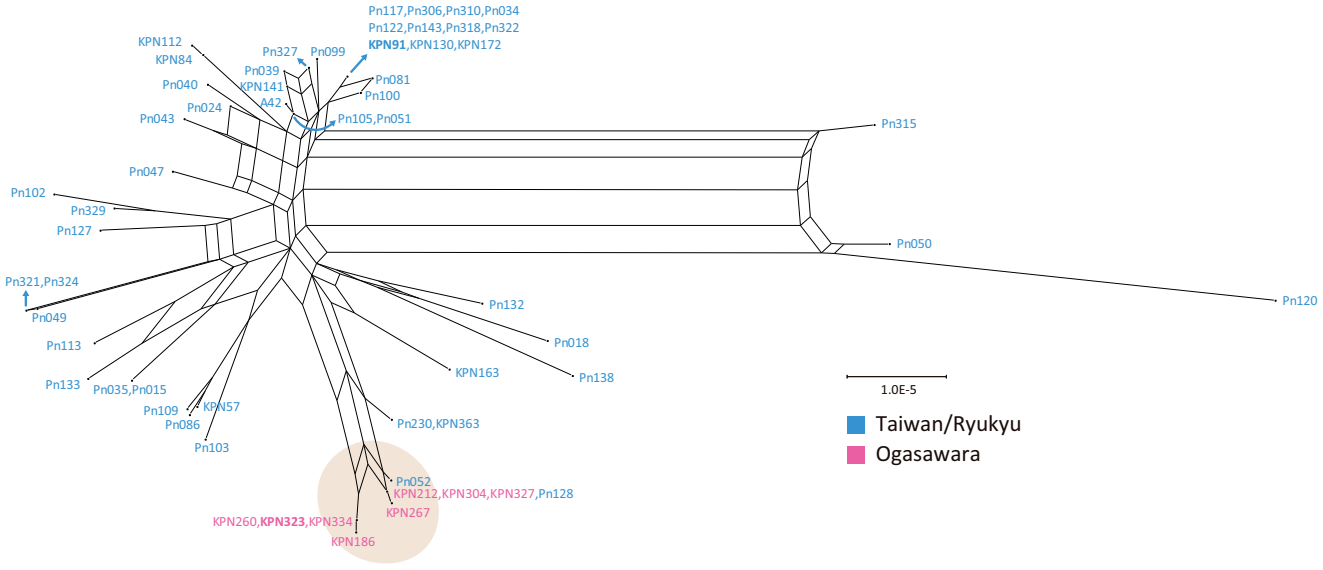

Fig. 5.—Neighbor-Net phylogenetic network of maximum-likelihood distance inferred from concatenated intronic sequences of 59 *Phellinus noxius* isolates.

alternatively code for lysine and arginine in these species. Two SNPs were observed in the 72-bp exon region resulting in two different alleles. In five isolates (Pn081, Pn102, Pn329, KPN141, and KPN163), a point mutation in the anticodon period turns the $tRNA^{Lys(CUU)}$ into an $tRNA^{Arg(CCU)}$, accompanying the translocation of surrounding sequences (supplementary fig. S7*C*, Supplementary Material online). The lysine tRNA was lost in four isolates (Pn015, Pn035, Pn086, and Pn127) due to a large fragment deletion (supplementary fig. S7*D*, Supplementary Material online), suggesting that it might be a nonessential tRNA and undergoing loss of gene.

Frequent Gain/Loss and Evidences of Rearrangements in Introns

Introns range from 57 to 61 in 9 intron-containing genes in 59 *P. noxius* isolates (supplementary fig. S5, Supplementary Material online). *Phellinus noxius* KPN91, which harbored most introns, had an exclusive group II intron of rnl_intron01 with an intact reverse transcriptase domain, suggesting the intron was recently acquired. Completely, loss of introns in some isolates was observed in five intron positions (cox1_intron04, cox1_intron06, cox1_intron07, rnl_intron02, and rnl_intron11). We constructed a phylogeny using the concatenated intronic sequences and showed incongruences to the one constructed based on whole genome variations where two genetical lineages (Taiwan/Ryukyu and Ogasawara) were defined (supplementary fig. S6, Supplementary Material online). To unravel the extent of conflicting signals in the sequences, we constructed a NN phylogenetic network (fig. 5), which is a form of split network where the presences of boxes suggest recombination between connected sequences (Bryant and Moulton 2004). Divergence of two lineages was indeed observed from the network as all eight isolates from Ogasawara island were grouped together. Extensive ambiguous phylogenetic signals were observed within the Taiwanese lineage. Evidence of inter-lineages rearrangements were found as two Taiwanese isolates (Pn052 and Pn128) were clustered together with the Ogasawara isolates and two more (Pn230 and KPN363) were located between the two lineages.

To further visualize the intron dynamics in the Taiwanese/Ryukyu lineage, we first chose one species from Taiwan/Ryukyu (KPN91) and Ogasarawa (KPN323) lineage as a reference and calculated nucleotide identity of all introns against these references. Intron identity of pairwise comparisons between two references is on average 97.1%, with 11 introns identical to each other. The intron with the lowest pairwise identity was rnl_intron12 with 41.8%, and a closer inspection revealed a unique double sized rnl_intron12. We plotted a heatmap of intron identity according to both references and revealed a mosaic pattern of intron distributions. With the double sized rnl_intron12, the introns of the two Taiwanese isolates that were clustered together to the Ogasawara lineage in the intron phylogeny resemble the introns of KPN323 more than that of KPN91 (fig. 6). In contrast, strains belonging to the Taiwan/Ryukyu lineage have revealed striking differences among strains (fig. 6). Three modes were found: 1) strains with introns that completely resemble the Taiwanese/Ryukyu reference, 2) strains with mosaic intron patterns that resemble either Taiwan/Ryukyu or Ogasawara references (i.e., Pn230 and KPN363), and 3) strains with introns that were equally dissimilar to both references. The strains showing the last mode were isolates that have the most ambiguous signals (as represented by boxes) in the NN

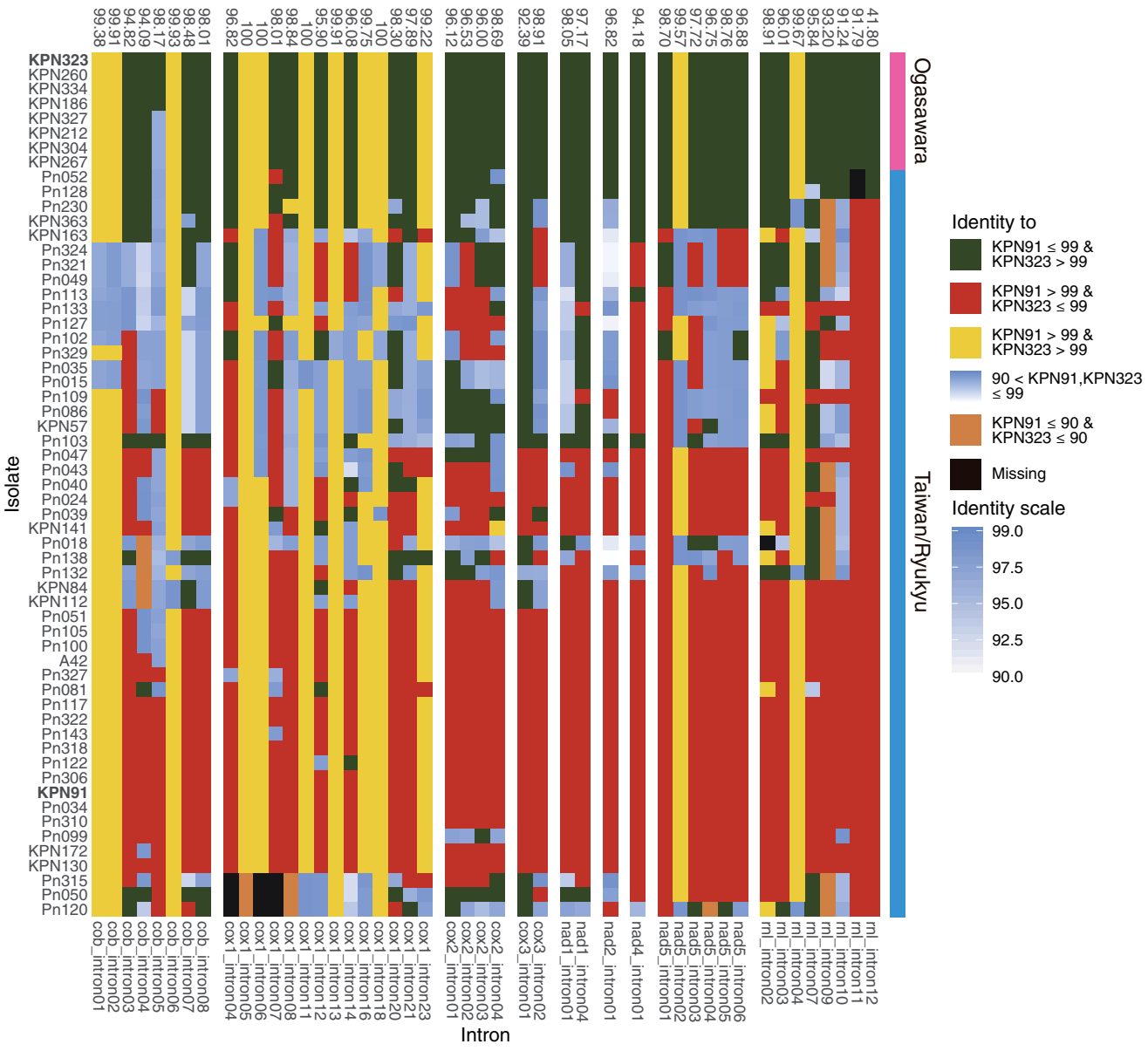

Fig. 6.—Heatmap of intron identity against KPN91 and KPN323. Intron positions with all identity >99% against KPN91 are removed. The numbers above the chart indicate the intron identity between KPN91 and KPN323. The tiles on the right of the chart are the lineages defined by intron pattern and intronic phylogeny. The *y* axis is the order of intronic phylogeny (supplementary fig. S6, Supplementary Material online).

phylogenetic network. The pattern is likely resulted from extensive recombinations between these isolates. Three Taiwanese isolates (Pn050, Pn120, and Pn315) were particularly distant to the rest of the isolates in the NN phylogenetic network. They showed distinct pattern in introns 4–8 of *cox1*, with two introns possessing low identity to other strains and absence of intronic sequences at three sites (fig. 6 and supplementary fig. S5, Supplementary Material online). These observations suggest that extensive rearrangement of introns have occurred in the Taiwan/Ryukyu lineage but less so in the Ogasawara lineage.

Evidence of Extensive Shuffling between Large Intergene Regions Separated by Gene Clusters

To understand the causes of large intergene that are present in *P. noxius*, we first defined three large (region 1: *nad4–rnl* 11.3–25.9 kb, region 2: *atp8–cox1* 15.3–35.4 kb, and region 3: *nad3–rns* 6.3–24.9 kb) and a small (region 4s: *cox2-cob* 4.6–8.9 kb) intergenic regions. A close species *P. lamaensis* had only 11.3 kb in the regions we defined, comparing to an average of 66.2 kb in *P. noxius*. MtDNA alignment also showed no similarity with other species in this study, suggesting that these intergenic

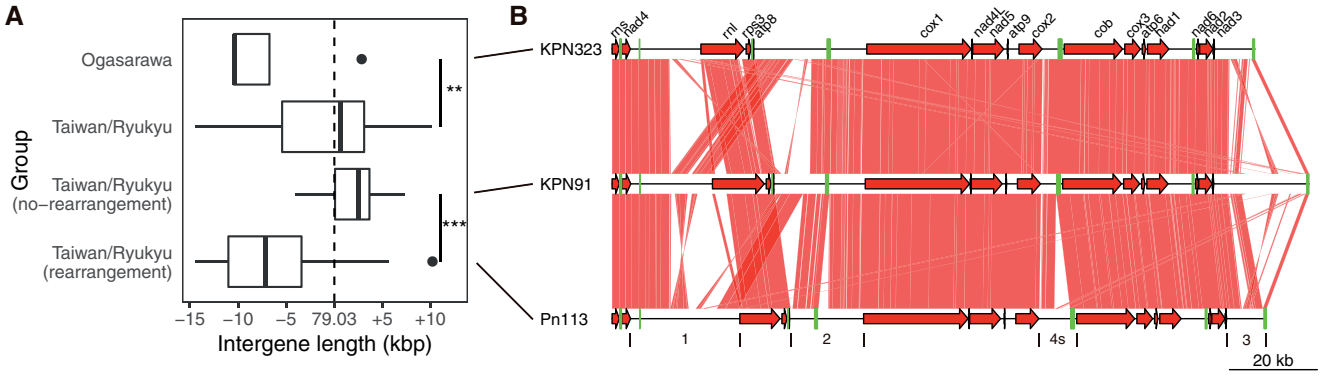

Fig. 7.—Intergene length distribution and rearrangement events between Ogasawara and Taiwan/Ryukyu lineages. (*A*) The intergene length between lineages and rearranged or nonrearranged intergene against KPN91 (supplementary fig. S10, Supplementary Material online) are significantly different (**$P < 0.01$ and ***$P < 0.001$). The dotted line represents KPN91 intergene length. (*B*) Rearrangement events in four defined regions between lineages in (*A*). Red arrows are mitochondrial core genes and green tiles are tRNA genes. Red links between mitogenomes are aligned regions with identity >80%. The intergene boundaries are labeled under Pn113. The plot was generated with genoplotR package in R.

regions are *P. noxius*-specific (supplementary fig. S2*B*, Supplementary Material online).

Frequent intra- and inter-rearrangements between four regions were observed. To validate the existence of rearrangement events, several primers at regions 1–3 were designed (supplementary table S4, Supplementary Material online). PCR for all valid primer combinations were successful and the product sizes were as expected, except two ultra-long PCR products (>13 kb for A1_F/B1_R on Pn113 and >20 kb for F1_F/C1_R on KPN323) due to technical limits (supplementary fig. S7, Supplementary Material online). We first sought if a correlation exists between the intron phylogeny and intergene. However, in the two distinct clades defined by the intron phylogeny, similar synteny was observed in isolates belonging to different clades (supplementary fig. S8*A* and *B*, Supplementary Material online). Pairwise identities of the concatenated intergenic sequences were then calculated between all isolates using two different metrics (supplementary fig. S9, Supplementary Material online). Using the gap-compressed identity, that is, not considering indels, isolates were grouped into two lineages where 11 isolates from Taiwan/Ryukyu lineage were also grouped with the Ogasawara isolates (supplementary fig. S9*A*, Supplementary Material online). In contrast, several isolates form distinct groups if indels were considered (supplementary fig. S9*B*, Supplementary Material online), suggesting that indels are major contributors to intergenic differences. Interestingly, these isolates were placed in the mosaic group in the intron network (figs. 5 and 6), implying evidences of rearrangement across mitogenomes of these isolates.

To investigate the effect of rearrangement in mitogenome evolution, we took KPN91 as a reference and sought if any rearrangement event occurred in the four defined intergenic regions (supplementary fig. S10, Supplementary Material online). All eight Ogasawara isolates had similar rearrangement pattern, and the intergene sizes were significantly shorter than that of Taiwan/Ryukyu isolates ($P < 0.01$; fig. 7). Isolates from the Taiwan/Ryukyu were subsequently classified into two groups based on intergene rearrangement pattern against KPN91 (supplementary fig. S10, Supplementary Material online), which were also significantly different in length ($P < 0.001$; fig. 7). The length of intergenic spacers in the isolates with rearrangement tended to be smaller than that of the isolates without rearrangement, resulting in a median difference of ~9.7 kb. On average, 22.17 breakpoints were defined in each isolate when compared with KPN91. To investigate whether these breakpoints were significantly enriched in repetitive regions at intergenes (9.73% in KPN91), we conducted a bootstrapping analysis and revealed observed breakpoints were significantly more commonly found in repeats than random. Out of 28 tested isolates with >10 breakpoints, 26 displayed significance (adjusted $P < 0.01$; supplementary table S3, Supplementary Material online), suggesting a strong association between rearrangement and repetitive elements at intergenes.

Discussion

In our previous study, we reported four *Hymenochaetales* genomes and revealed the nature of hyperdiversity of nuclear genomes in two lineages of *P. noxius* in Taiwan and Japan areas (Chung et al. 2015; Chung et al. 2017). To understand the mitochondrial genomics in *Hymenochaetales*, we analyzed six mitogenomes in this order. All mitogenomes can be circularized, indicating the high quality of these assemblies. All fungal mitochondrial core genes are present in these species, and the synteny are largely conserved according to their phylogenetic relationships. The overlapping start and stop codons of *nad* genes have been observed in not only fungi but also animals (Franco et al. 2017; Wang et al. 2019),

presumably because of the mRNA transcription of these genes has remained coupled across independent lineages. Only tRNAs were found duplicated and lost, presumably due to the preference of mitochondrial recombination in these regions (Fritsch et al. 2014).

The six mitogenomes varied by at most 3.6-fold in length, from 45.6 kb in *P. lamaensis* to 163.4 kb in *P. noxius*. In Organelle Genome Resources NCBI, only six species are larger than *P. noxius* (Losada et al. 2014; Mardanov et al. 2014; Kanzi et al. 2016; Nowrousian 2016). Gain of introns have been depicted as the main constituents of the enlargement of fungal mitogenomes (Losada et al. 2014; Mardanov et al. 2014; Salavirta et al. 2014; Kanzi et al. 2016). In the case of *Hymenochaetales*, three out of the six species hold an impressively high number of introns (table 1). In particular, *cox1* harbors up to 23 introns in these species which is consistent to previous surveys in fungal mitogenomes as the most intron-containing gene.

Horizontal gene transfer event has been implicated as the main causes and origins of intron gains in fungi (Hausner 2012; Wu et al. 2015). We determined 39 out of 65 shared intron positions, however, only 14 and 3 intron sites were shared in more than 2 or 3 species, respectively. From these sites, we found only two examples of shared intron exhibiting same phylogenetic relationship as the species tree, implying an ancient transposition event. Additional evidence from comparative analysis of multiple species within an order will help reveal whether the retention of such introns has any selective advantage.

Intergenic regions constitute the majority of mitogenomes in all species in this study, consistent with previous findings in yeast mitogenomes where intergenic sequences played a role in genome expansion (Xiao et al. 2017). The initial expansion of intergenic regions may be contributed by the integration of plasmid-like sequences since the few numbers of repetitive elements (Hausner 2003; Férandon et al. 2013). Unlike the introns which need to be spliced precisely for mature mRNA, the integrated plasmid sequences are easily degenerated overtime due to the absence of selection pressure (Hausner 2003; Swithers et al. 2009). Integration of invertron plasmid in mtDNA has been reported in many fungi species including *Moniliophthora perniciosa*, *A. bisporus*, and *Sclerotinia borealis* (Formighieri et al. 2008; Férandon et al. 2013; Mardanov et al. 2014). We found at least one family B DNA polymerase located in intergenic regions in all six species (table 1), but no putative RNA polymerase or invertron-like repetitive elements, suggesting degenerated integrated plasmid.

Our previous investigation on population-scale sequencing of *P. noxius* nuclear genomes suggests that it is a hypervariable species. Hence, one of the aims of this study was to investigate the evolution history of *P. noxius* from the mitochondrial perspective. Surprisingly, the analysis of 59 isolates revealed different pace of evolution across coding, intronic, and intergenic regions. The coding regions unusually harbor low variation across the two lineages, suggesting strong purifying selection, that is, arising substitutions were quickly purged from the population. Considering the much higher mutation rate in mitogenome than the nuclear genome (Jung et al. 2012), additional regulatory mechanisms may exist in hypervariable species to reduce potential detrimental effects from the replication of mitogenome. An exception is that a $tRNA^{Lys(CUU)}$ between *nad4* and *rnl* found deleted in several isolates (supplementary fig. S8*C* and *D*, Supplementary Material online). *Phellinus noxius* mitogenome uses the AAG codon at a very low frequency (<2%) to code for lysine. The lack of mitochondria-encoded tRNA is pretty common across all eukaryotes and may be compensated via different wobble rules, RNA-editing or import from cytoplasm (Salinas-Giegé et al. 2015).

A previous investigation of intraspecific variations on three species of yeast determined introns contributed the highest variance in genome size (Xiao et al. 2017). Our intron analyses of two lineages of *P. noxius* revealed high similarity but extensive rearrangements of introns among strains of different clades. Our results add up to the expanding list of basidiomycete mitogenomes that have displayed evidences of hybridization and recombination (Xu et al. 2009; Wang et al. 2017). There are two possible scenarios that can account for such observations in a basidiomycete during hyphal fusion between strains of two mitotypes: intron homing or homologous recombination (Haugen et al. 2005; Wu et al. 2015; Leducq et al. 2017). We observed fewer gain and loss of introns at population level so recombination may be a more predominant process, which has been documented in various fungal species (Leducq et al. 2017). Unfortunately, high similarity of intron sequences impedes further recombination-detection based analyses. Future investigations should focus on determination of mitochondrial inheritance mode and the frequency and mechanisms involved in intron rearrangements using artificial hybrids.

In plants (Sloan et al. 2012) and animals (Marlétaz et al. 2017), huge intraspecific variations in intergenic regions have been documented as extremes or unusual atypical to mitogenome evolution. Such large intraspecific variations appear to be more common in fungi which were observed in our investigation, *Cryptococcus* (Litter et al. 2005; Xu et al. 2009) and other closely related fungal species (Burger et al. 2003; Aguileta et al. 2014; Himmelstrand et al. 2014). We have observed contrasting differences in intergene length between strains of different lineages as well as within a lineage. These findings suggest that, when compared with closely related species, intergene variations are currently driving intraspecific mitogenomic variation in *P. noxius* and may eventually lead to larger intergene variations. The absolute difference in intergene length led to presence of additional sequences in some strains. Possible origins of these sequences may be a result of horizontal

gene transfer (gain), or rearrangement and accumulations of mutations (gain or loss). It is challenging to determine which scenario as these sequences share no homology to publicized genomes. We speculate the later scenario may be more likely as repeats were found associated with rearrangement events identified within the strains of Taiwan/Ryukyu lineage. Intriguingly, these strains were found to possess introns with evidences of rearrangements. Similar extents of rearrangement were reported across the Dikarya and have led to gene order differences (Aguileta et al. 2014; Li et al. 2018). Recombination, break-induced replication (Christensen 2013) coupled with repeats and several nuclear genes (Shedge et al. 2007; Arrieta-Montiel et al. 2009) and accelerated mitochondrial mutation rate have all been proposed to explain the evolution of noncoding sequences in mitogenomes. It remains to be determined how repeats contribute to intergenic rearrangement and expansion without perturbing gene order in mitogenome of *P. noxius*.

In conclusion, we have revealed frequent rearrangements at intergenic regions play a major role in shaping and extending the mtDNA in Basidiomycetes at inter- and intra-species level. The extreme contrast between nuclear genome and coding region of mitogenome suggests strong purifying selection acting on these genes. Basidiomycetes can be excellent models in understanding mtDNA inheritance. A comprehensive sampling and detailed comparison across mitogenomes will help delineate the relationship between mating and mitochondrial diversity.

Supplementary Material

Supplementary data are available at *Genome Biology and Evolution* online.

Author Contributions

I.J.T. conceived the study. H.-M.K., C.-Y.I.L., T.J.L., and C.-L.C. established the strains collection, carried out experiments, and sequencing. H.-H.L. carried out comparative analysis. I.J.T. and H.-H.L. wrote the manuscript. This work was supported by Academia Sinica of Taiwan (AS-CDA-107-L01 to I.J.T) and Taiwan Ministry of Science and Technology (Grant No. 105-2628-B-001-002-MY3 to IJT). T.J.L was supported by the doctorate fellowship of Taiwan International Graduate Program-Biodiversity, Academia Sinica of Taiwan. C.-L.C was supported by the Office of General Affairs, National Taiwan University.

Literature Cited

Aguileta G, et al. 2014. High variability of mitochondrial gene order among fungi. Genome Biol Evol. 6(2):451–465.

Akiba M, et al. 2015. Genetic differentiation and spatial structure of *Phellinus noxius*, the causal agent of brown root rot of woody plants in Japan. PLoS One 10(10):e0141792.

Ann P-J, Chang T-T, Ko W-H. 2002. *Phellinus noxius* brown root rot of fruit and ornamental trees in Taiwan. Plant Dis. 86(8):820–826.

Arrieta-Montiel MP, Shedge V, Davila J, Christensen AC, Mackenzie SA. 2009. Diversity of the *Arabidopsis* mitochondrial genome occurs via nuclear-controlled recombination activity. Genetics 183(4):1261–1268.

Basse CW. 2010. Mitochondrial inheritance in fungi. Curr Opin Microbiol. 13(6):712–719.

Benson G. 1999. Tandem repeats finder: a program to analyze DNA sequences. Nucleic Acids Res. 27(2):573–580.

Berger KH, Yaffe MP. 2000. Mitochondrial DNA inheritance in *Saccharomyces cerevisiae*. Trends Microbiol. 8(11):508–513.

Bryant D, Moulton V. 2004. Neighbor-Net: an agglomerative method for the construction of phylogenetic networks. Mol Biol Evol. 21(2):255–265.

Bullerwell CE, Leigh J, Forget L, Lang BF. 2003. A comparison of three fission yeast mitochondrial genomes. Nucleic Acids Res. 31(2):759–768.

Burger G, Gray MW, Franz Lang B. 2003. Mitochondrial genomes: anything goes. Trends Genet. 19(12):709–716.

Capella-Gutierrez S, Silla-Martinez JM, Gabaldon T. 2009. trimAl: a tool for automated alignment trimming in large-scale phylogenetic analyses. Bioinformatics 25(15):1972–1973.

Casselton LA, Kües U. 2007. The origin of multiple mating types in the model mushrooms *Coprinopsis cinerea* and *Schizophyllum commune*. In: Heitman J, Kronstad JW, Taylor JW, Casselton LA, editors. Sex in fungi: molecular determination and evolutionary implications. Washington: American Society of Microbiology. p. 283–300.

Christensen AC. 2013. Plant mitochondrial genome evolution can be explained by DNA repair mechanisms. Genome Biol Evol. 5(6):1079–1086.

Chung C-L, et al. 2015. The genetic structure of *Phellinus noxius* and dissemination pattern of brown root rot disease in Taiwan. PLoS One 10(10):e0139445.

Chung C-L, et al. 2017. Comparative and population genomic landscape of *Phellinus noxius*: a hypervariable fungus causing root rot in trees. Mol Ecol. 26(22):6301–6316.

de la Bastide PY, Horgen PA. 2003. Mitochondrial inheritance and the detection of non-parental mitochondrial DNA haplotypes in crosses of *Agaricus bisporus* homokaryons. Fungal Genet Biol. 38(3):333–342.

Deng Y, et al. 2018. Comparison of the mitochondrial genome sequences of six *Annulohypoxylon stygium* isolates suggests short fragment insertions as a potential factor leading to larger genomic size. Front Microbiol. 9:380.

Dierckxsens N, Mardulyn P, Smits G. 2017. NOVOPlasty: de novo assembly of organelle genomes from whole genome data. Nucleic Acids Res. 45(4):e18.

Dobin A, et al. 2013. STAR: ultrafast universal RNA-seq aligner. Bioinformatics 29(1):15–21.

Edgar RC. 2004. MUSCLE: a multiple sequence alignment method with reduced time and space complexity. BMC Bioinformatics 5:113.

Fedler M, Luh K-S, Stelter K, Nieto-Jacobo F, Basse CW. 2009. The *a2* mating-type locus genes *lga2* and *rga2* direct uniparental mitochondrial DNA (mtDNA) inheritance and constrain mtDNA recombination during sexual development of *Ustilago maydis*. Genetics 181(3):847–860.

Férandon C, Xu J, Barroso G. 2013. The 135 kbp mitochondrial genome of *Agaricus bisporus* is the largest known eukaryotic reservoir of group I introns and plasmid-related sequences. Fungal Genet Biol. 55:85–91.

Finn RD, et al. 2016. The Pfam protein families database: towards a more sustainable future. Nucleic Acids Res. 44(D1):D279–D285.

Floudas D, et al. 2012. The Paleozoic origin of enzymatic lignin decomposition reconstructed from 31 fungal genomes. Science 336(6089):1715–1719.

Formighieri EF, et al. 2008. The mitochondrial genome of the phytopathogenic basidiomycete *Moniliophthora perniciosa* is 109 kb in size and contains a stable integrated plasmid. Mycol Res. 112(Pt 10): 1136–1152.
Franco MEE, et al. 2017. The mitochondrial genome of the plant-pathogenic fungus *Stemphylium lycopersici* uncovers a dynamic structure due to repetitive and mobile elements. PLoS One 12(10):e0185545.
Fritsch ES, Chabbert CD, Klaus B, Steinmetz LM. 2014. A genome-wide map of mitochondrial DNA recombination in yeast. Genetics 198(2):755–771.
Haugen P, Simon DM, Bhattacharya D. 2005. The natural history of group I introns. Trends Genet. 21(2):111–119.
Hausner G. 2003. Fungal mitochondrial genomes, plasmids and introns. In: Arora DK, Khachatourians GG, editors. Fungal Genomics. Amsterdam: Elsevier. p. 101–131.
Hausner G. 2012. Introns, mobile elements, and plasmids. Berlin/Heidelberg (Germany): Springer. p. 329–357.
Hawksworth DL, Lücking R. 2017. Fungal diversity revisited: 2.2 to 3.8 million species. Microbiol Spectr.5(4).
Hepting GH. 1971. Diseases of forest and shade trees of the United States. Washington (DC): U.S. Department of Agriculture Forest Service.
Himmelstrand K, Olson Å, Durling MB, Karlsson M, Stenlid J. 2014. Intronic and plasmid-derived regions contribute to the large mitochondrial genome sizes of *Agaricomycetes*. Curr Genet. 60(4):303–313.
Hintz W, Anderson JB, Horgen PA. 1988. Nuclear migration and mitochondrial inheritance in the mushroom *Agaricus bitorquis*. Genetics 119(1):35–41.
Jin T, Horgen PA. 1993. Further characterization of a large inverted repeat in the mitochondrial genomes of *Agaricus bisporus* (=*A. brunnescens*) and related species. Curr Genet. 23(3):228–233.
Jin T, Horgen PA. 1994. Uniparental mitochondrial transmission in the cultivated button mushroom, *Agaricus bisporus*. Appl Environ Microbiol. 60(12):4456–4460.
Jung PP, Friedrich A, Reisser C, Hou J, Schacherer J. 2012. Mitochondrial genome evolution in a single protoploid yeast species. G3 (Bethesda) 2:1103–1111.
Kalyaanamoorthy S, Minh BQ, Wong TKF, von Haeseler A, Jermiin LS. 2017. ModelFinder: fast model selection for accurate phylogenetic estimates. Nat Methods. 14(6):587–589.
Kanzi AM, Wingfield BD, Steenkamp ET, Naidoo S, van der Merwe NA. 2016. Intron derived size polymorphism in the mitochondrial genomes of closely related *Chrysoporthe* species. PLoS One 11(6):e0156104.
Katoh K, Standley DM. 2013. MAFFT multiple sequence alignment software version 7: improvements in performance and usability. Mol Biol Evol. 30(4):772–780.
Krzywinski MI, et al. 2009. Circos: an information aesthetic for comparative genomics. Genome Res. 19(9):1639–1645.
Kurtz S, et al. 2004. Versatile and open software for comparing large genomes. Genome Biol. 5(2):R12.
Laslett D, Canbäck B. 2004. ARAGORN, a program to detect tRNA genes and tmRNA genes in nucleotide sequences. Nucleic Acids Res. 32(1):11–16.
Leducq J-B, et al. 2017. Mitochondrial recombination and introgression during speciation by hybridization. Mol Biol Evol. 34(8):1947–1959.
Li H. 2018. Minimap2: pairwise alignment for nucleotide sequences. Bioinformatics 34(18):3094–3100.
Li Q, et al. 2018. Comparative mitogenomics reveals large-scale gene rearrangements in the mitochondrial genome of two *Pleurotus* species. Appl Microbiol Biotechnol. 102:6143–6153.
Litter J, Keszthelyi A, Hamari Z, Pfeiffer I, Kucsera J. 2005. Differences in mitochondrial genome organization of *Cryptococcus neoformans* strains. Antonie Van Leeuwenhoek 88(3-4):249–255.
Losada L, et al. 2014. Mobile elements and mitochondrial genome expansion in the soil fungus and potato pathogen *Rhizoctonia solani* AG-3. FEMS Microbiol Lett. 352(2):165–173.
Lowe TM, Chan PP. 2016. tRNAscan-SE On-line: integrating search and context for analysis of transfer RNA genes. Nucleic Acids Res. 44(W1):W54–W57.
Mardanov AV, Beletsky AV, Kadnikov VV, Ignatov AN, Ravin NV. 2014. The 203 kbp mitochondrial genome of the phytopathogenic fungus *Sclerotinia borealis* reveals multiple invasions of introns and genomic duplications. PLoS One 9(9):e107536.
Marlétaz F, Le Parco Y, Liu S, Peijnenburg K. 2017. Extreme mitogenomic variation in natural populations of Chaetognaths. Genome Biol Evol . 9(6):1374–1384.
McGinnis S, Madden TL. 2004. BLAST: at the core of a powerful and diverse set of sequence analysis tools. Nucleic Acids Res. 32(Web Server issue):W20–W25.
Min B, et al. 2015. Genome sequence of a white rot fungus *Schizopora paradoxa* KUC8140 for wood decay and mycoremediation. J Biotechnol. 211:42–43.
Mullineux S-T, Costa M, Bassi GS, Michel F, Hausner G. 2010. A group II intron encodes a functional LAGLIDADG homing endonuclease and self-splices under moderate temperature and ionic conditions. RNA 16(9):1818–1831.
Nguyen L-T, Schmidt HA, von Haeseler A, Minh BQ. 2015. IQ-TREE: a fast and effective stochastic algorithm for estimating maximum-likelihood phylogenies. Mol Biol Evol. 32(1):268–274.
Nowrousian M. 2016. Complete mitochondrial genome sequence of the Pezizomycete *Pyronema confluens*. Genome Announc. 4(3):e107536.
Sahashi N, Akiba M, Ishihara M, Ota Y, Kanzaki N. 2012. Brown root rot of trees caused by *Phellinus noxius* in the Ryukyu Islands, subtropical areas of Japan. For Pathol. 42(5):353–361.
Salavirta H, et al. 2014. Mitochondrial genome of *Phlebia radiata* is the second largest (156 kbp) among fungi and features signs of genome flexibility and recent recombination events. PLoS One 9(5):e97141.
Salinas-Giegé T, Giegé R, Giegé P. 2015. tRNA biology in mitochondria. Int J Mol Sci. 16(3):4518–4559.
Sandor S, Zhang Y, Xu J. 2018. Fungal mitochondrial genomes and genetic polymorphisms. Appl Microbiol Biotechnol. 102(22):9433–9448.
Shedge V, Arrieta-Montiel M, Christensen AC, Mackenzie SA. 2007. Plant mitochondrial recombination surveillance requires unusual *RecA* and *MutS* homologs. Plant Cell 19(4):1251–1264.
Sloan DB, Müller K, McCauley DE, Taylor DR, Storchová H. 2012. Intraspecific variation in mitochondrial genome sequence, structure, and gene content in *Silene vulgaris*, an angiosperm with pervasive cytoplasmic male sterility. New Phytol. 196(4):1228–1239.
Soorni A, Haak D, Zaitlin D, Bombarely A. 2017. Organelle_PBA, a pipeline for assembling chloroplast and mitochondrial genomes from PacBio DNA sequencing data. BMC Genomics. 18(1):49.
Swithers KS, Senejani AG, Fournier GP, Gogarten JP. 2009. Conservation of intron and intein insertion sites: implications for life histories of parasitic genetic elements. BMC Evol Biol. 9:303.
Thiel T, Michalek W, Varshney R, Graner A. 2003. Exploiting EST databases for the development and characterization of gene-derived SSR-markers in barley (*Hordeum vulgare*). Theor Appl Genet. 106(3):411–422.
Toor N, Zimmerly S. 2002. Identification of a family of group II introns encoding LAGLIDADG ORFs typical of group I introns. RNA 8(11):1373–1377.
Untergasser A, et al. 2012. Primer3—new capabilities and interfaces. Nucleic Acids Res. 40(15):e115.
Voelz K, et al. 2013. Transmission of hypervirulence traits via sexual reproduction within and between lineages of the human fungal pathogen *Cryptococcus gattii*. PLoS Genet. 9(9):e1003771.

Walker BJ, et al. 2014. Pilon: an integrated tool for comprehensive microbial variant detection and genome assembly improvement. PLoS One 9(11):e112963.
Wang L, Zhang S, Li J-H, Zhang Y-J. 2018. Mitochondrial genome, comparative analysis and evolutionary insights into the entomopathogenic fungus *Hirsutella thompsonii*. Environ Microbiol. 20(9):3393–3405.
Wang P, et al. 2017. Frequent heteroplasmy and recombination in the mitochondrial genomes of the basidiomycete mushroom *Thelephora ganbajun*. Sci Rep. 7(1):1626.
Wang Z, Wilson A, Xu J. 2015. Mitochondrial DNA inheritance in the human fungal pathogen *Cryptococcus gattii*. Fungal Genet Biol. 75:1–10.
Wang Z, et al. 2019. The complete mitochondrial genome of *Parasesarma pictum* (Brachyura: Grapsoidea: Sesarmidae) and comparison with other Brachyuran crabs. Genomics. 111(4):799–807.
Wheeler DL, et al. 2003. Database resources of the National Center for Biotechnology. Nucleic Acids Res. 31(1):28–33.
Wilson AJ, Xu J. 2012. Mitochondrial inheritance: diverse patterns and mechanisms with an emphasis on fungi. Mycology 3(2):158–166.
Wolf K, Burger G, Lang B, Kaudewitz F. 1976. Extrachromosomal inheritance in *Schizosaccharomyces pombe*. I. Evidence for an extrakaryotically inherited mutation conferring resistance to antimycin. Mol Gen Genet. 144(1):67–73.
Wolters JF, Chiu K, Fiumera HL. 2015. Population structure of mitochondrial genomes in *Saccharomyces cerevisiae*. BMC Genomics. 16:451.
Wu B, Buljic A, Hao W. 2015. Extensive horizontal transfer and homologous recombination generate highly chimeric mitochondrial genomes in yeast. Mol Biol Evol. 32(10):2559–2570.
Wu TD, Watanabe CK. 2005. GMAP: a genomic mapping and alignment program for mRNA and EST sequences. Bioinformatics 21(9):1859–1875.
Xiao S, Nguyen DT, Wu B, Hao W. 2017. Genetic drift and indel mutation in the evolution of yeast mitochondrial genome size. Genome Biol Evol. 9(11):3088–3099.
Xu J, He L. 2015. Current perspectives on mitochondrial inheritance in fungi. Cell Health and Cytoskelet. 7:143–112.
Xu J, Wang P. 2015. Mitochondrial inheritance in basidiomycete fungi. Fungal Biol Rev. 29(3-4):209–219.
Xu J, Yan Z, Guo H. 2009. Divergence, hybridization, and recombination in the mitochondrial genome of the human pathogenic yeast *Cryptococcus gattii*. Mol Ecol. 18(12):2628–2642.
Xu J, Zhang Y, Pun N. 2013. Mitochondrial recombination in natural populations of the button mushroom *Agaricus bisporus*. Fungal Genet Biol. 55:92–97.
Xu J, et al. 2000. Uniparental mitochondrial transmission in sexual crosses in *Cryptococcus neoformans*. Curr Microbiol. 40(4):269–273.
Yan Z, Xu J. 2003. Mitochondria are inherited from the *MAT*a parent in crosses of the basidiomycete fungus *Cryptococcus neoformans*. Genetics 163(4):1315–1325.
Yan Z, et al. 2018. Deletion of the sex-determining gene *SXI1α* enhances the spread of mitochondrial introns in *Cryptococcus neoformans*. Mob DNA 9:24.
Zhu P, Zhai B, Lin X, Idnurm A. 2013. Congenic strains for genetic analysis of virulence traits in *Cryptococcus gattii*. Infect Immun. 81(7):2616–2625.

Associate editor: Jason Stajich